Energies **2013**, *6*, 4980-5002; doi:10.3390/en6104980

OPEN ACCESS

energies

ISSN 1996-1073

www.mdpi.com/journal/energies

Article

Investigation of a Novel 24-Slot/14-Pole Six-Phase Fault-Tolerant Modular Permanent-Magnet In-Wheel Motor for Electric Vehicles

Ping Zheng [1,*], Fan Wu [1], Yu Lei [2], Yi Sui [1] and Bin Yu [1]

[1] Department of Electrical Engineering, Harbin Institute of Technology, Harbin 150080, China; E-Mails: wufan871226@126.com (F.W.); suiyi_hitee2005@163.com (Y.S.); yubin1983@163.com (B.Y.)

[2] North China Electric Power Research Institute, Beijing 100045, China; E-Mail: heaven_hit@163.com

* Author to whom correspondence should be addressed; E-Mail: zhengping@hit.edu.cn; Tel./Fax: +86-451-8640-3086.

Received: 17 July 2013; in revised form: 10 September 2013 / Accepted: 22 September 2013 / Published: 26 September 2013

Abstract: In this paper, a six-phase fault-tolerant modular permanent magnet synchronous machine (PMSM) with a novel 24-slot/14-pole combination is proposed as a high-performance actuator for wheel-driving electric vehicle (EV) applications. Feasible slot/pole combinations of the fractional-slot concentrated winding six-phase PMSM are elicited and analyzed for scheme selection. The novel 24-slot/14-pole combination is derived from the analysis and suppression of the magnetomotive force (MMF) harmonics. By making use of alternate-teeth-wound concentrated winding configuration, two adjacent coils per phase and unequal teeth widths, the phase windings of the proposed machine is magnetically, thermally isolated, which offers potentials of modular design and fault tolerant capability. Taking advantage of the leakage component of winding inductance, 1.0 per unit short-circuit current is achieved endowing the machine with short-circuit proof capability. Optimal design of essential parameters aiming at low eddy current losses, high winding factor and short-circuit-proof ability are presented to pave the way for a high-quality system implementation.

Keywords: fractional-slot concentrated winding; harmonic analysis; multiphase PMSM; modular machine; in-wheel motor

---

1. Introduction

Multiphase fault-tolerant permanent magnet (PM) in-wheel motors, equipped with alternated-teeth-wound fractional-slot concentrated windings (FSCWs), are quite promising candidates in applications of four-wheel-driving electric vehicles (EVs) attributing to their high torque density, high efficiency and high fault-tolerant capability [1–3]. By employing excessive winding redundancy over three phases, the stator winding of the multiphase PM machine can keep on forming the circulating rotating magnetic field when a fault occurs in one or even more phases. By making use of neodymium-iron-boron (NdFeB) rotor PMs with high remanence, coercivity and energy product, the power density of the machine is superior to existing fault-tolerant alternating current (AC) machines such as switched reluctance motor, flux switching machine and doubly salient machines [4–6], which makes it prevalent in this field throughout the past years.

For the design principle of fault-tolerant PM machines, electrical, magnetic, thermal, physical isolation features are listed as the most essential ones [7,8]. These isolation features aim to eliminate any impact induced by the faulty winding upon the remaining phases, so as to provide a reliable transition to the stage of post-fault control and continuous operation. The fractional-slot concentrated winding machines, in which the stator windings are non-overlapped and wrapped around all teeth or alternate teeth, cater to the requirement of the above isolation features [9–11]. Especially, by employing the alternate-teeth-wound fractional-slot concentrated windings, the coils are alternatively wound around the stator teeth, which provides an advantage of thermal isolation and physical isolation of the stator phase windings [12,13]. The electrical isolation feature can be achieved by making use of the full-bridge inverter topology manipulating the phase voltages rather than the line-to-line voltages [14,15]. Such machines have relatively large self-inductance and small mutual inductance assuring that the faulty winding will not affect the healthy ones. Furthermore, a close slot/pole combination of the fractional-slot concentrated winding machine, *i.e.*, $2p$ (pole number) = Q (slot number) ± 2, should be utilized in order to maximize the flux linkage and torque density [16,17]. Hence, a high winding factor of more than 0.9 and negligible cogging torque can also be obtained.

Under the above type of slot/pole combinations, the winding-produced main magnetomotive force (MMF) component, which is defined as the component whose wavelength equals the pole pitch [18], is normally a high-order one while other low-order and higher-order components exist leading to a larger harmonic leakage inductance compared to that of the conventional distributed winding configurations. The numerical calculation methods for the leakage inductances are mentioned in references [19,20]. Since the rotating speed of the harmonic component is reversely proportional to its order, the lowest-order one is at the maximum spin speed in a relative movement to the rotor PMs. Consequently, the eddy currents induced in the PMs are rather considerable. Segmentation technique that circumferentially and axially separates the PMs into blocks is often applied to deal with the issue [21,22]. By doing that, the fabrication process gets tougher since the PM blocks repel one another. Ways to cope with the MMF harmonic components should be sought.

With the development of the theory of fractional-slot concentrated winding, the modular design concept has been introduced to the design of fractional-slot concentrated winding machines, in which the stator windings can be constructed with separated armature cores [23]. A modular three-phase 18-slot/12-pole scheme formed with 18 stator armature core modules was used in the Honda Civic

hybrid electric vehicle (HEV) with the advantages of short end winding and easy fabrication. For fault-tolerant purpose, such a kind of stator construction offers convenience for replacement when the winding in a module suffers a failure, thus reducing the maintenance costs. A five-phase five-slot/six-pole fault-tolerant modular PM prototype machine with five soft magnetic composite (SMC)-constructed modules was investigated for safety-critical applications [24,25]. It is found that the SMC modules suffered cracks during the fabrication process with a non-uniform air gap left after assembly. More importantly, neither the phase windings of the *m*-phase/*m*-slot nor those of the other existing PM modular machines are completely magnetically isolated, which means that they are physically modularized but not magnetically.

This paper starts out with the analysis of feasible slot/pole combinations for the six-phase fault-tolerant fractional-slot concentrated winding machines. To solve the problem of high iron loss and temperature rise of rotor PMs due to excessive MMF harmonic components, several machine schemes including 24-slot/22-pole alternate-teeth-wound scheme, 24-slot/22-pole all-teeth-wound scheme, *etc.*, are discussed and compared. A novel alternate-teeth-wound 24-slot/14-pole symmetric six-phase fault-tolerant permanent-magnet in-wheel motor is proposed and investigated. To advance the value of the winding pitch factor of the proposed machine, alternate-teeth-wound fractional-slot concentrated winding with unequal stator teeth widths are applied. With two adjacent coil per phase and excellent magnetically isolation features, it is suitable for the proposed machine to adopt the modular design conception for easy fabrication and post-fault operation. Besides, the outer rotor prototype machine is designed and optimized aiming at high power/torque density.

2. Scheme Selection of the Six-Phase Fault-Tolerant Permanent Magnet Synchronous Machine (PMSM)

2.1. Winding Arrangements and Feasible Slot/Pole Combinations

On winding phase belt level, there are two schemes for the six-phase permanent magnet machines, *i.e.*, symmetric six-phase PMSM with 60 degree phase belt and asymmetric six-phase PMSM with 30 degree phase belt, as shown in Figure 1.

Figure 1. Two winding configurations for six-phase permanent magnet synchronous machine (PMSM): (**a**) symmetric six-phase PMSM; and (**b**) asymmetric six-phase PMSM.

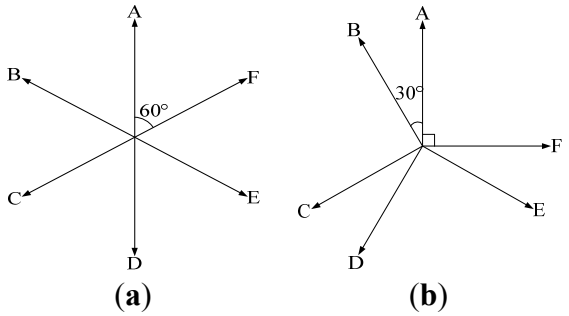

(**a**) (**b**)

The symmetric six-phase PMSM has similar magnetic features referring to a 60-degree phase-belt three-phase PMSM [26]. On the other hand, the asymmetric six-phase PMSM [27], with two three-phase windings shifting by 30 degree, is magnetically approximate to a twelve-phase machine. Thus, it can

be called a semi-twelve-phase PMSM [28]. Apparently, one of the differences between the two schemes is the winding-produced MMF harmonic components. The MMF harmonic components of the asymmetric six-phase PMSM is $(12k \pm 1)$th, and that of the symmetric six-phase PMSM is $(6k \pm 1)$th. Roughly speaking, the MMF harmonic components of the asymmetric six-phase PMSM are almost half of that of the symmetric one. There is no doubt that the asymmetric six-phase PMSM might have less iron loss and lower torque ripple. However, the situation depends on not only the numbers of harmonics but also the amplitudes of harmonics that should be discussed in specific situations.

It is known to all that, the flux linkage will enhance with a close slot and pole numbers, and thus, a high torque density is achieved. Based on that viewpoint, the machine used for direct-driving EV applications is proposed to employ slot and pole combinations satisfied with $2p = Q \pm 2$, where p denotes the pole number and Q denotes the slot number. The feasible slot and pole combinations are listed in Tables 1 and 2, where LCM denotes the lowest common multiple of slot and pole numbers; *SPP* denotes slot number per pole per phase. And, a larger LCM number indicates a lower cogging torque. Both alternate-teeth-wound and all-teeth-wound fractional-slot concentrated windings are taken into consideration.

Table 1. Possible slot/pole combinations of the symmetric six-phase PMSM equipped with fractional-slot concentrated windings (FSCWs). Notes: ▲ means the combinations enable alternate-teeth-wound design.

Q	$2p$	$\|Q-2p\|$	LCM	Winding type	k_w	*SPP*	Notes
6	4	2	12	All-teeth-wound	0.866	1/2	-
	8	2	24	All-teeth-wound	0.866	1/4	-
12	10	2	60	Alternate-teeth-wound	0.933	2/5	▲
				All-teeth-wound			-
	14	2	84	Alternate-teeth-wound	0.933	2/7	▲
				All-teeth-wound			-
18	16	2	144	All-teeth-wound	0.945	3/8	-
	20	2	180	All-teeth-wound	0.945	3/10	
24	22	2	264	Alternate-teeth-wound	0.949	2/11	▲
				All-teeth-wound			-
	26	2	312	Alternate-teeth-wound	0.949	2/13	▲
				All-teeth-wound			-
30	28	2	420	All-teeth-wound	0.951	5/14	-
	32	2	480	All-teeth-wound	0.951	5/16	-
36	34	2	612	Alternate-teeth-wound	0.956	6/17	▲
				All-teeth-wound			-
	38	2	684	Alternate-teeth-wound	0.956	6/19	▲
				All-teeth-wound			-
42	40	2	840	All-teeth-wound	0.965	7/20	-
	44	2	924	All-teeth-wound	0.965	7/22	-
48	46	2	1104	Alternate-teeth-wound	0.989	4/23	▲
				All-teeth-wound			-
	50	2	1200	Alternate-teeth-wound	0.989	4/25	▲
				All-teeth-wound			-
$6k$	$6k \pm 2$	2	-	-	-	-	-

Table 2. Possible slot/pole combinations of the asymmetric six-phase PMSM equipped with FSCWs. Notes: ■ means the combinations enable alternate-teeth-wound design and have highest winding factor.

Q	$2p$	$\|Q-2p\|$	LCM	Winding type	k_w	SPP	Notes
24	22	2	264	Alternate-teeth-wound	0.991	2/11	■
				All-teeth-wound			-
	26	2	312	Alternate-teeth-wound	0.991	2/13	■
				All-teeth-wound			-
48	46	2	1104	Alternate-teeth-wound	0.989	4/23	-
				All-teeth-wound			-
	50	2	1200	Alternate-teeth-wound	0.989	4/25	-
				All-teeth-wound			-
$24k$	$24k \pm 2$	2	-	-	-	-	-

Although the pole and slot combinations have been introduced in the discussion of six-phase supply feasibility, the selections for the feasible six-phase supply are limited to two three-phase winding shifting by 30 degree [29]. However, in Tables 1 and 2, two possible winding distributions—symmetric and asymmetric six-phase windings—are involved with the limitation of $2p = Q \pm 2$. With the design of close slot and pole numbers, there are more combinations for the symmetric six-phase PMSM as shown in Tables 1 and 2.

As shown in Table 1, only the schemes with $12k$ slot numbers allow the alternate-teeth-wound winding arrangements (marked with ▲). With alternate-teeth-wound windings, the machine is well protected against internal short-circuit failure between phases. The winding factor increases and cogging torque decreases when the slot and pole numbers get larger. Among all the slot/pole combinations shown in Tables 1 and 2, the 24-slot/22-pole or 24-slot/26-pole asymmetric six-phase scheme (marked with ■), which enables alternate-teeth-wound winding arrangement and has the largest winding factors, is more suitable for the in-wheel applications than the others.

Additionally, compared to symmetric six-phase PMSM, the winding axes of asymmetric six-phase PMSM are not coincident with each other, which enables a fault tolerance up to four-phase open circuit fault. For instance, assume that the open circuit fault occurs at the phases A, B, D and E in Figure 1b, the symmetric six-phase machine merely has two aligned phases C and F. Thus, it is impossible to reconstruct a circular rotating MMF field in some types of severe fault conditions.

2.2. MMF Harmonic Analysis

In this paper, the MMF harmonic is represented by an integer harmonic system rather than a fractional harmonic system. For a fractional-slot concentrated winding machine, the main component of the stator MMF is commonly a high-order component instead of the 1st component [18]. Thus, the harmonic leakage inductance is quite large compared to the conventional distributed winding machine. Furthermore, the harmonics of the stator MMF have impacts on the cogging torque, eddy-current loss and power factor. Among all the MMF harmonic components, the two-pole sub-harmonic component [22] which travels at a reverse different speed is particularly high. MMF harmonic analysis is performed to compare schemes with different winding arrangements and slot/pole combinations.

As mentioned earlier in Section 2.1, the 24-slot/22-pole (or 24-slot/26-pole) asymmetric six-phase scheme, which enables alternate-teeth-wound winding arrangement and has the largest winding factors, is more suitable for the applications. The winding arrangement and MMF harmonic analysis are shown in Figure 2, based on the MMF calculation theorem for concentrated winding machines [30]. The MMF harmonic spectrum is obtained by analyze the winding-produced air-gap flux density.

Figure 2. Winding arrangement and main magnetomotive force (MMF) harmonic analysis of the 24-slot alternate-teeth-wound asymmetric six-phase PMSM: (**a**) stator winding arrangement and synthesized electromotive force (EMF) vector; (**b**) air-gap flux density; and (**c**) winding-produced air-gap flux density spectrum.

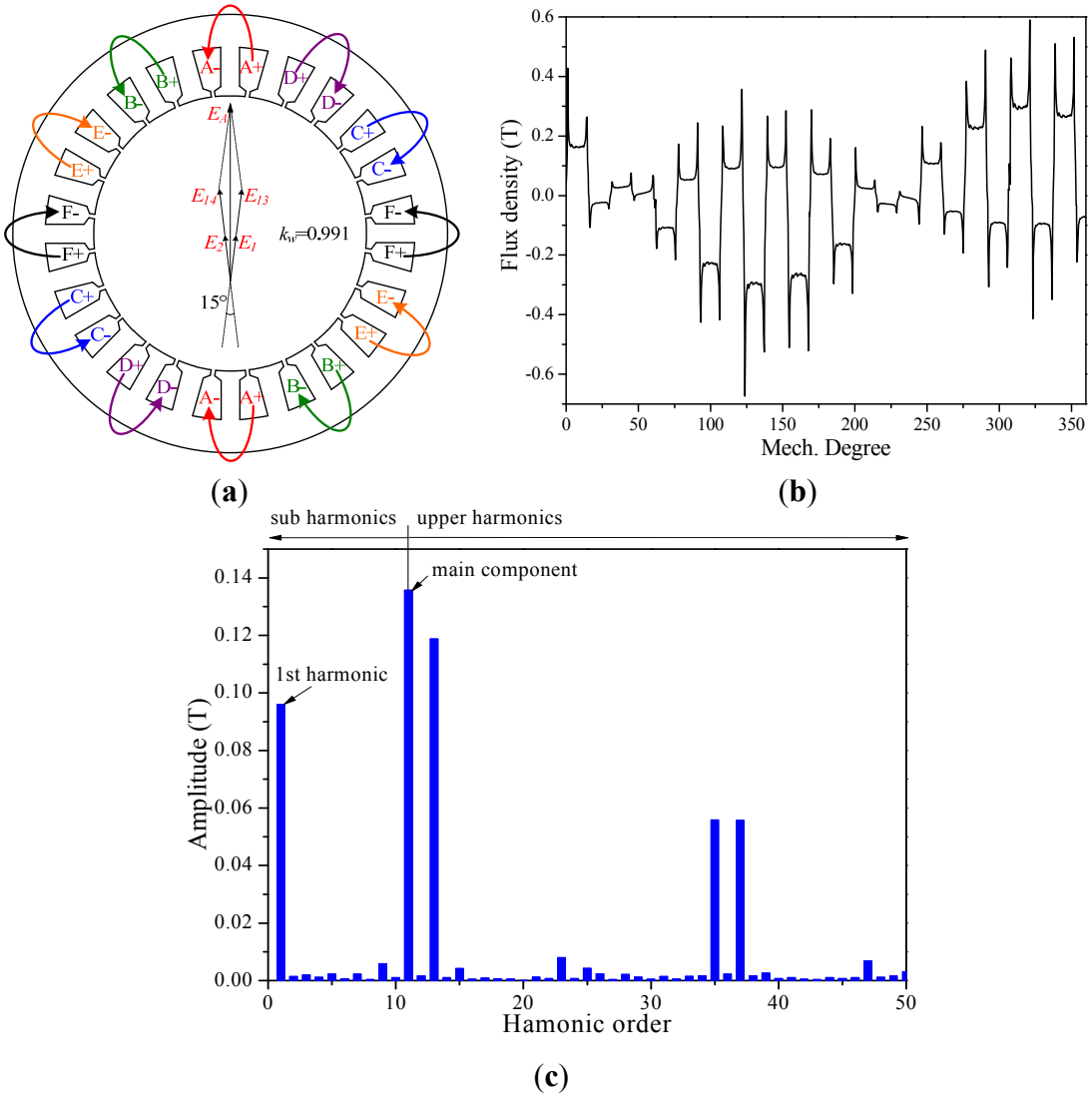

As can be seen in Figure 2c, the spectrum of the flux density produced by the stator windings consists of (12k ± 1)th harmonic components. Also, a strong 1st component can be observed with amplitude of 70.4% of the main component (11th). Thus it induces eddy current both in iron and PMs, which is determined by the amplitude and velocity contrast [31]. Such a large harmonic content can drastically reduce the motor performance. Specifically, it can reduce the power factor and efficiency,

and cause temperature rises in the PMs. To solve this problem, all-teeth-wound schemes are frequently employed, as shown in Figure 3.

Figure 3. Winding arrangement and MMF harmonic analysis of the 24-slot all-teeth-wound asymmetric six-phase PMSM: (**a**) stator winding arrangement and the synthesized EMF vector; (**b**) air-gap flux density; and (**c**) winding-produced air-gap flux density spectrum.

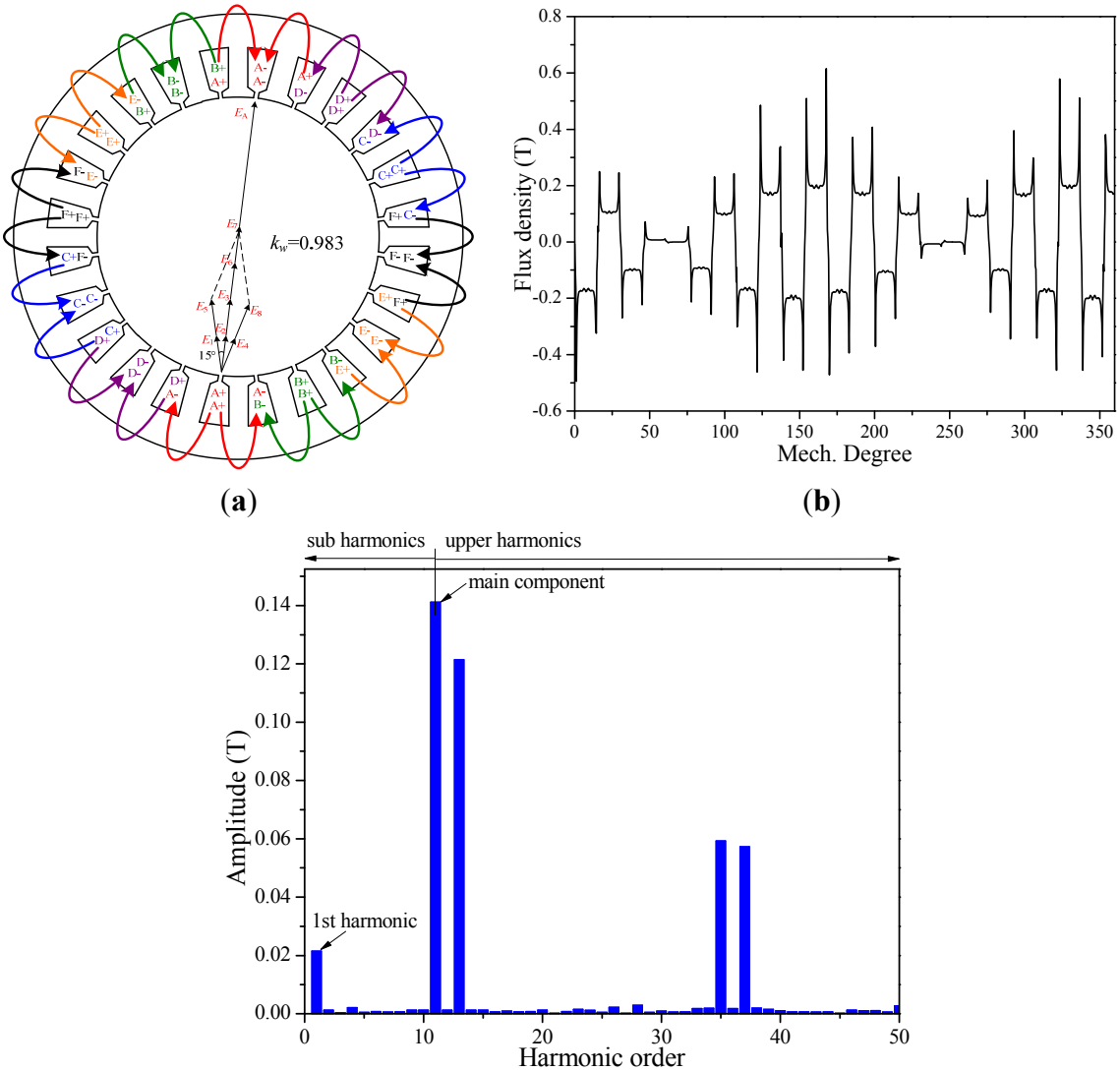

The 24-slot/22-pole all-teeth-wound scheme changes the distributing winding factor of each harmonic component. It can be clearly seen that, the 1st component is prominently suppressed. By making use of the estimation formula illustrated in reference [32], the PM losses produced by the 1st harmonic are reduced by 95.01% attributing to a change from alternate-teeth-wound scheme to all-teeth-wound scheme. However, as for fault-tolerant drives, isolation between the phase windings is of great significance. Note that each slot of the above scheme contains two coil sides. Thus, there are possibilities of short-circuit failure between phases, which increases the probability of failures that are difficult to deal with. Hence, the challenge becomes how to suppress the 1st MMF harmonic with alternate-teeth-wound windings. One possible solution is presented in Figure 4.

Figure 4. Stator winding arrangements of the 24-slot alternate-teeth-wound six-phase PMSM: (**a**) two coils of same phase shifting by 150 degree; (**b**) two adjacent coils per phase; and (**c**) two adjacent coils per phase with unequal teeth widths.

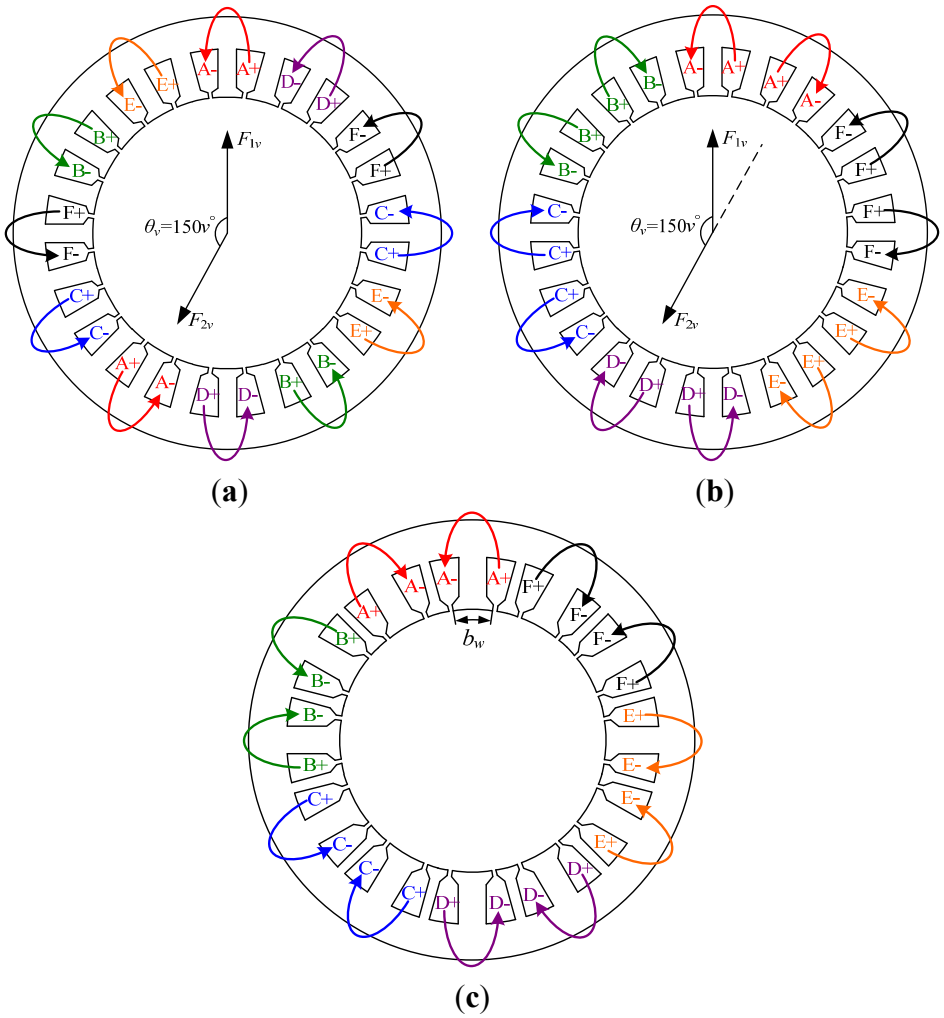

As can be seen in Figure 4a, the idea begins with employing two coils of the same phase shifting by 150 mechanical degree in order to change the distributed factor of the stator MMF vectors. The angle θ_v = 150v° in Figure 4a denotes the electrical angle between two MMF vectors F_{1v} and F_{2v} for the vth MMF harmonic component. Thus, the synthetized MMF vectors for the vth harmonic component are given by:

$$\vec{F}_v = \vec{F}_{1v} + \vec{F}_{2v} = 2\vec{F}_{mv}\cos(v75^\circ) = 2\vec{F}_{mv}K_{dv} \quad (1)$$

where the F_{mv} denotes the amplitude of the 1st MMF component; K_{dv} = cos(v75°) is defined to be the distributed factor for vth MMF component and calculated in Table 3, which indicates the suppression level of the harmonics.

Table 3. The distributed factor for vth MMF component.

Harmonic order	1st	5th	7th	11th	13th	17th	19th	23th	25th	[6(2k + 1) ± 1]th	(12k ± 1)th
K_{dv}	0.259	0.966	−0.966	0.259	−0.259	0.966	−0.966	0.259	−0.259	±0.966	±0.259
$\|K_{dv}\|$	0.259	0.966	0.966	0.259	0.259	0.966	0.966	0.259	0.259	0.966	0.259

It can be clearly seen from Table 3 that, such a kind of winding arrangement pattern suppresses the 1st, 11th, 13th… MMF harmonic components effectively, while the 5th, 7th… components remain nearly unchanged. Furthermore, the two coils of one phase can be placed adjacent to each other as shown in Figure 4b without transferring the relationship between the MMF vectors established in Figure 4a. Therefore, the winding-produced flux can close within a short path so that a better magnetic isolation features can be achieved. And, the winding-produced air-gap flux density and MMF spectrum for the scheme shown in Figure 4b is illustrated in Figure 5.

Figure 5. MMF harmonic analysis of the 24-slot asymmetric six-phase PMSMs having two adjacent coils per phase and equal teeth widths: (**a**) winding-produced air-gap flux density; and (**b**) spectrum.

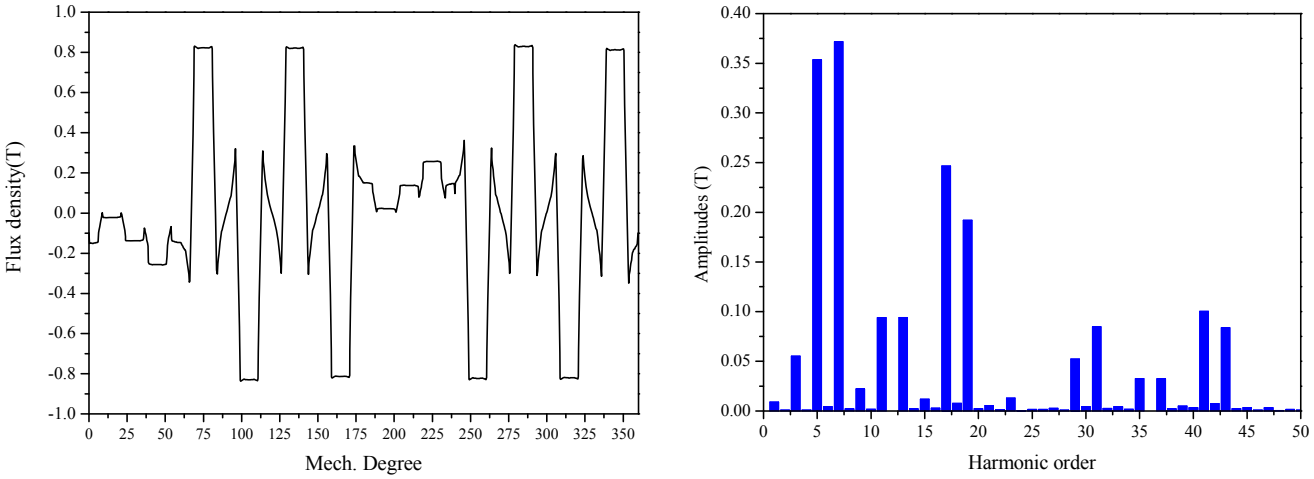

(**a**) (**b**)

As can be seen in Figure 5, the 1st harmonic component of the MMF has been nearly eliminated while the fifth and seventh component has become the predominant MMF components amid the air-gap flux density spectrum. Consequently, the appropriate number of rotor poles should be 10 or 14 instead of 22 or 26, resulting in a specific 24-slot/10-pole or 24-slot/14-pole combination. With the decreased number of rotor poles, the pole pitch for the stator winding is much less than 1, which leads to a smaller pitch factor. The pitch factor for the *h*th harmonic component is given by:

$$K_p = \sin\left(h\frac{b_w}{b_{eq}}\frac{\pi}{Q}\right) \tag{2}$$

where b_w is the coil-wound tooth tip span which is specified in Figure 4c; b_{eq} is the tooth tip span when all tooth tip spans are equal; and Q is the slot number. Therefore, unequal tooth tip spans could be employed to enlarge the pitch span of the winding to advance winding pitch factor, as shown in Figure 4c. Since the pole pitch of a 14-pole scheme is shorter than that of a 10-pole scheme and the maximum teeth span for the 24-slot scheme can be 1/12 of the circumferential length, it is only feasible to adopt a 24-slot/14-pole scheme. The air-gap flux density and spectrum are shown in Figure 6 regarding a 24-slot/14-pole symmetric six-phase PMSMs having two adjacent coils per phase and unequal teeth width.

As shown in Figure 6, by making use of the extended coil-wound tooth span, the 5th and 7th harmonic components become more dominant among all the MMF components compared with what is shown in Figure 5b.

Figure 6. MMF harmonic analysis of the 24-slot symmetric six-phase PMSMs having two adjacent coils per phase and unequal teeth widths: (**a**) winding-produced air-gap flux density; and (**b**) spectrum.

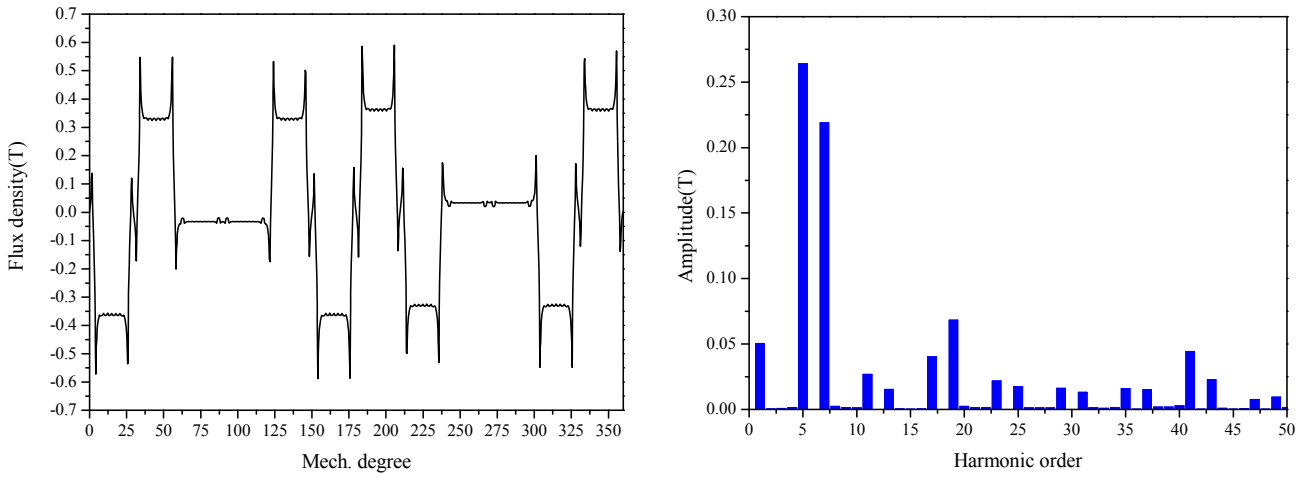

(**a**) (**b**)

Imagine that the widths of the non-wound tooth tips are adjusted to be zero, the 24-slot/14-pole machine will actually transform into a 12-slot/14-pole one with all-teeth-wound windings. Here we provide the differences between the two schemes to clarify this point:

(1) The all-teeth-wound 12-slot/14-pole scheme allows the underlying possibility of short-circuit fault between two different phases, which means that the scheme is not electrically isolated and inappropriate for fault-tolerant uses;

(2) Referring to a winding short-circuit failure, the non-wound teeth play a role that provides the closest path for the flux linked by the short-circuit winding. Thus, the fault will not interfere the remaining phases as the other alternate-teeth-wound schemes did.

Additionally, some references have already focused on concentrated winding machines using an irregular distribution of the slots [33–35]. Even though the irregular distribution of the slots is, essentially, the unequal teeth scheme, it can still be distinguished from what is talking in this article. What is concerned in references [33–35] is how the irregular distribution of the slots is derived from a conventional distributed winding step by step. Besides, high performances—reduced copper loss, low torque ripple and enhanced output torque—was obtained by employing the structure of irregular slot distribution. However, in our paper, the 24-slot/14-pole machine is derived from a 24-slot/22-pole machine (both of them are fractional-slot concentrated winding machines). The major concern is that whether the new pattern can suppress the MMF harmonics and achieve a better isolation feature.

3. Machine Design

3.1. Modular Design of the Stator

Although the modular design conception has been introduced to the *m*-phase/2*m*-slot alternate-teeth-wound fractional-slot concentrated winding machinery series, in which the stator can be divided into several E-shape modules each consisting of one full tooth, its wrapped coil and two incomplete teeth, the phase windings are not magnetically isolated [36]. Another fact is that the fit tolerances between the separated stator armature cores are inevitable during manufacturing process. Therefore, the magnetic resistance will be increased in the stator yoke, affecting the torque capability of the machine. The flux lines in the six-phase 12-slot modular machinery series are shown in Figure 7. It is obviously that the flux lines produced by the winding of the six-phase 12-slot modular machine will go long paths in the stator yoke. Hence, this kind of machines is not suitable for modular design.

Figure 7. The winding-produced flux distribution of a six-phase/12-slot modular PMSM.

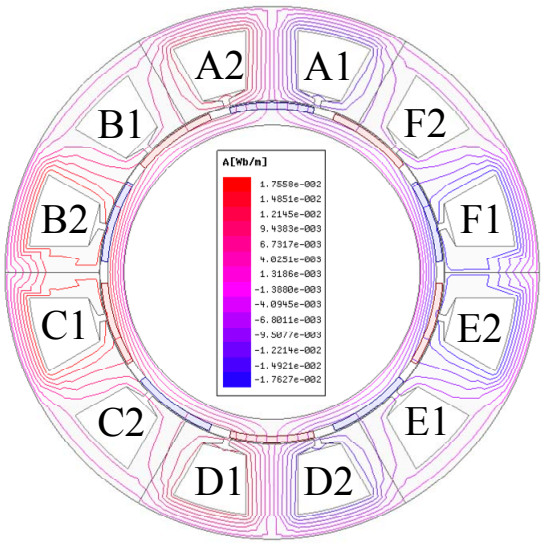

With two adjacent coils per phase and excellent magnetic isolation feature, it is more convenient for the proposed 24-slot/14-pole machine to adopt a modular design concept for easy fabrication and post-fault replacement. The stator modules can be constructed both from SMC or lamination stack. It is found that, the lamination-steel-sheet constructed modules are more suitable for a low-speed high-torque machine. In contrast, the SMC modules are suitable for a high-speed low-torque machine since the iron losses can be prominently reduced by employing SMC materials [37].

The divided stator core wound with concentric winding simplifies the construction of the stator and reduces the end winding loss. Moreover, it offers a convenience in maintenance that the faulty core can be readily substituted for a new one. Thus, the cost of maintenance is reduced.

The 24-slot/14-pole six-phase modular PMSM is shown in Figure 8. As can be seen in Figure 8a, the stator of the 24-slot/14-pole six-phase PMSM is made up of six modules. Semi-circular grooves are applied in the modules to assemble the separated armature cores together to form the whole stator. As shown in Figure 8b, each module consists of two alternate-teeth-wound four slot concentric coils. Besides, two half teeth are located in both two ends of the module.

Figure 8. The 24-slot/14-pole modular six-phase PMSM: (**a**) segment-stator 24-slot/14-pole PMSM; and (**b**) modular armature core.

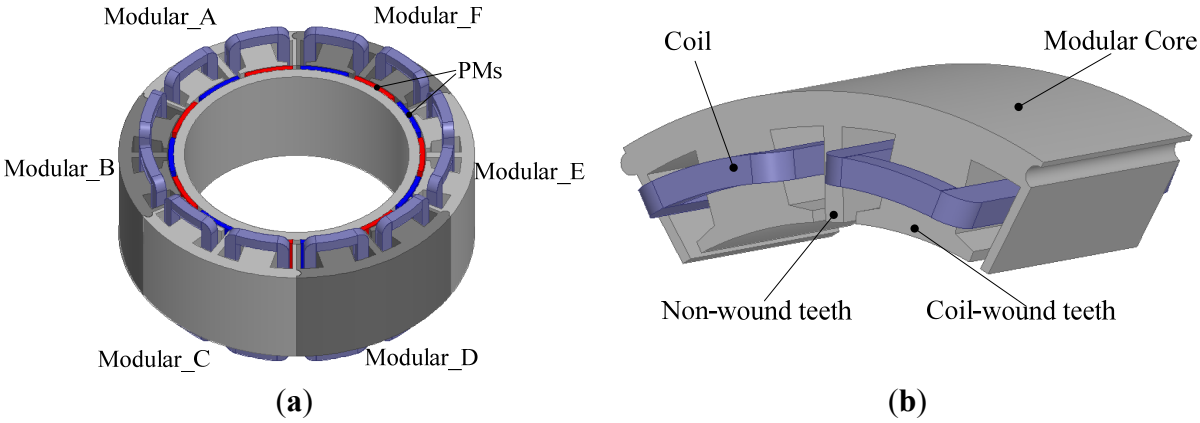

(**a**) (**b**)

3.2. Finite Element Method (FEM)-Based Design and Optimization

The alternate-teeth-wound 24-slot/14-pole scheme with unequal teeth widths is presented and proposed to be a promising candidate for improving the reliability of EV driving system, as mentioned in the above sections. For in-wheel application, an original model of the outer rotor 24-slot/14-pole scheme is established with Ansoft Maxwell 2-D Design, as shown in Figure 9a. And the key parameters and dimensions are listed in Table 4.

Figure 9. Original finite element model of the outer rotor 24-slot/14-pole scheme: (**a**) model; and (**b**) mesh plot.

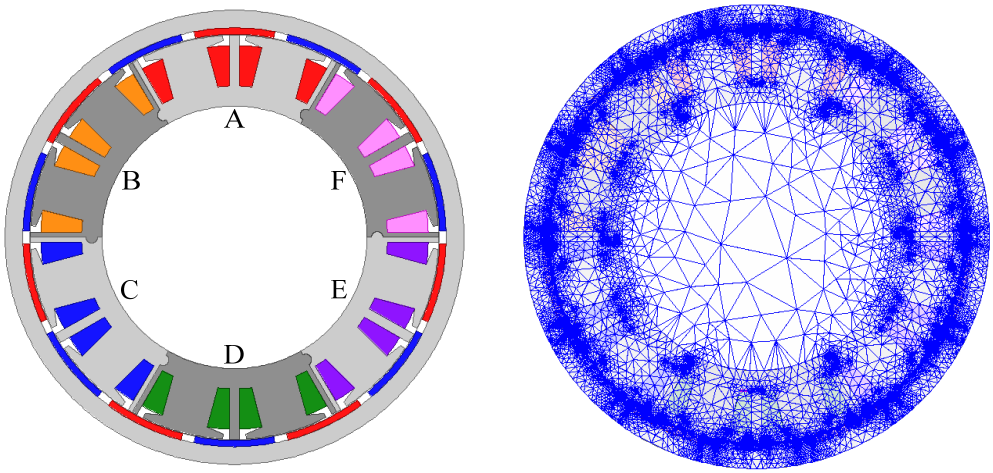

(**a**) (**b**)

The flux density distribution and winding-produced flux lines of the original design are shown in Figure 10a,b based on transient 2-D simulation, respectively. As shown in Figure 10a, the maximum flux density in stator yoke, stator teeth and teeth tips are 1.70T, 1.68T and 2.1T, respectively, aiming to take full use of the material and pursue high power density. As can be seen in Figure 10b, since the flux produced by a phase winding closes in a short path within the modular it belongs to except for some leakage components, the six modules are well magnetically isolated.

Table 4. Key parameters and dimensions of the original design.

Parameters	Units	Values
Inner diameter of stator	mm	208
Outer diameter of stator	mm	320
Outer diameter of rotor	mm	360
Air gap length	mm	1
Slot opening	mm	5
Stack length	mm	45
Magnet height	mm	5
Pole arc coefficient	-	0.8
Material of PMs	-	N45SH (B_r = 1.35T)
Maximum current	Arms	21.22
Current density	A/mm^2	10.05
Slot fill factor	%	72.1%
Number of conductors per slot		102
Maximum torque@450 rpm	Nm	250.85
1st component of back EMF@450 rpm	V	132
Rated/Maximum output power	kW	12/24
Active power-to-mass density	kW/kg	1.257
Efficiency (@450 rpm, with maximum torque and i_d = 0 control)	%	92.3

Figure 10. Flux density distribution and flux lines@450 rpm with rated load: (**a**) flux density map; and (**b**) winding-produced flux lines.

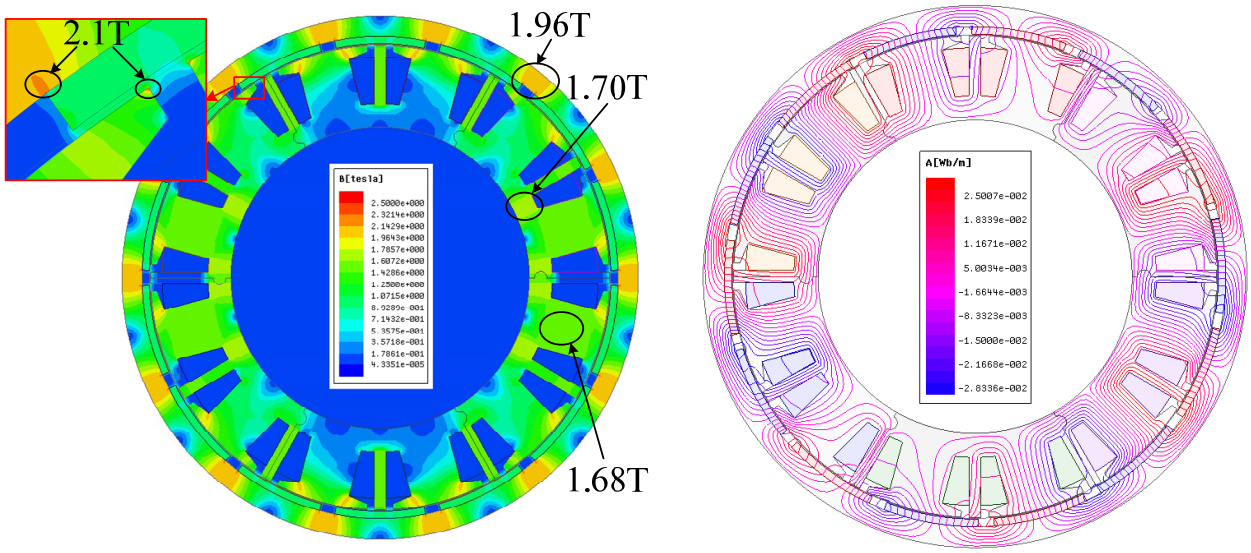

(**a**) (**b**)

The torque behaviors achieved by the above transient 2-D simulation are shown in Figure 11a,b including the cogging torque and rated torque. The maximum value of the cogging torque is 2.62 Nm as can be seen in Figure 11a with open circuit operation. As shown in Figure 11b, the average torque is 250.85 Nm with torque ripple of 5.83%.

Figure 11. Torque behavior@450 rpm: (**a**) cogging torque with on load; and (**b**) rated torque with $i_d = 0$ control.

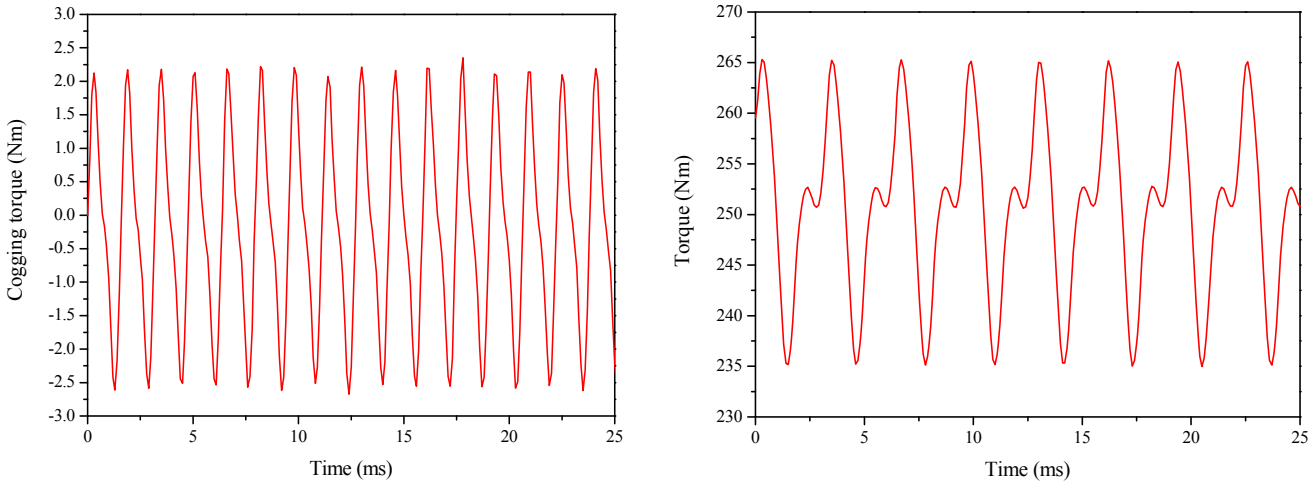

(**a**) (**b**)

The back EMF waveform and spectral analysis are shown in Figure 12. As can be seen in Figure 12a, the back EMFs in the six-phase windings of the 24-slot/14-pole machine are presented with a duty cycle of 19.05 ms and a sequent electrical angle shift of 60 degree from phase A to F. The maximum value of the back electromotive force (EMF) during the period is 114.88 V. From the spectrum analysis illustrated in Figure 12b, we can see that the main harmonic component of the back EMF waveform comprises the 3rd, 5th, 9th and 11th harmonics. The total harmonic distortion (THD) of the back EMF waveform is 17.8%.

Figure 12. Back EMF waveform@450 rpm: (**a**) six-phase back EMF; and (**b**) spectrum for the back EMF in phase A.

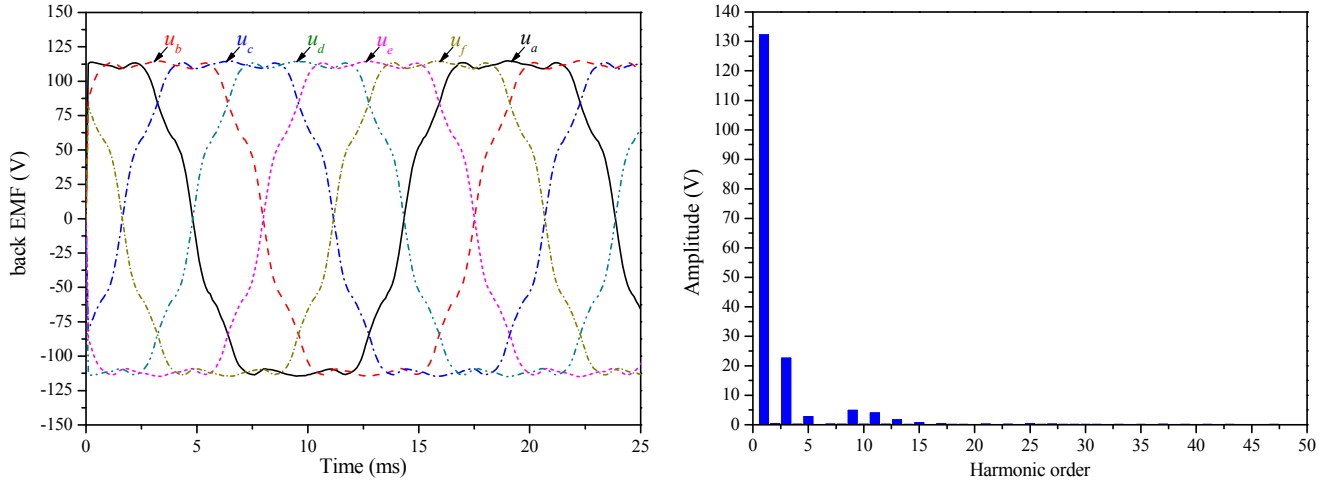

(**a**) (**b**)

As mentioned in Section 2, the span of coil-wound teeth tips should be increased to advance the pitch factor of the proposed 24-slot/14-pole machine. All the dimensions of the machine model are fixed except for the span of coil-wound teeth tip to search for the optimal value. The impact of the

tooth tip span upon the cogging torque and back EMF are shown in Table 5 and Figure 13, in which the tooth tip span is represented using the circumferential angle and broadened from 18° to 20.5°.

Table 5. Cogging torque and harmonic components of back EMF.

Teeth tip span	Cogging torque (Nm)	1st (V)	3rd (V)	5th (V)	7th (V)	9th (V)	11th (V)	13th (V)	15th (V)
18°	3.96	137.77	20.2	1.16	1.13	3.36	1.99	0.230	0.455
18.5°	6.25	139.37	16.1	0.160	0.883	3.40	2.41	0.278	0.306
19°	6.80	140.70	12.5	0.850	0.558	3.24	2.48	0.346	0.166
19.5°	5.61	141.87	10.1	1.84	0.166	2.81	2.22	0.375	0.150
20°	2.66	142.85	9.14	2.82	0.314	2.14	1.67	0.418	0.233
20.5°	1.63	143.65	8.54	3.72	0. 853	1.29	0.845	0. 432	0.261

Figure 13. Performance varies with different span of coil-wound teeth tip: (**a**) cogging torque; and (**b**) spectrum for the back EMFs in all phases.

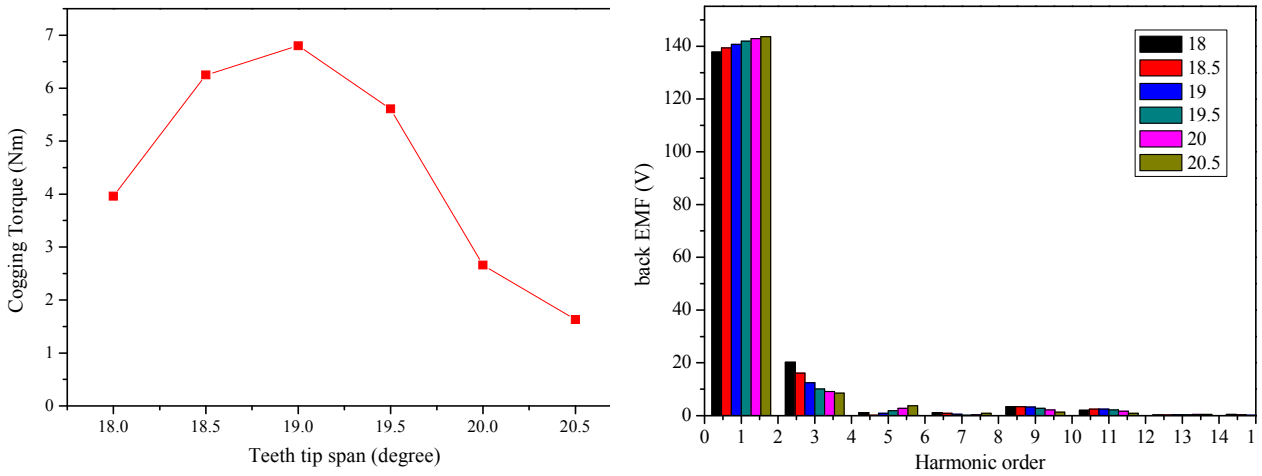

(**a**) (**b**)

As can be seen in Figure 13a, the cogging torque reaches a maximum value of 6.80 Nm with the tooth tip span of 19°, and a minimum value of 1.63 Nm with the tooth tip span of 20.5°. For the back EMF spectrums shown in Figure 13b, the 1st component of the back EMF is slightly increased with the tooth tip span gets wider. The main harmonic components, *i.e.*, 3rd, 5th, 9th and 11th, remain at low levels. And there is a downtrend for the 3rd, 9th and 11th harmonic components and an uptrend for the 5th one. The optimal tooth tip span of the coil-wound tooth is 20.5°.

The pole arc coefficient also affects the performances of the machine. The pole arc coefficient is varies from 0.5 to 0.9 to see the impact on the cogging torque and back EMF harmonics, as shown in Table 6 and Figure 14.

As can be seen in Figure 14a, the cogging torque reaches a minimum of 1.72 Nm with the pole arc coefficient of 0.75. However, a lower pole arc coefficient results in a lower power density. Thus, we choose a high pole arc coefficient of 0.9 to obtain a high power density design.

Table 6. Cogging torque and harmonic components of back EMF.

Pole arc coefficient	Cogging torque (Nm)	1st (V)	3rd (V)	5th (V)	7th (V)	9th (V)	11th (V)	13th (V)	15th (V)
0.5	6.92	124.90	2.22	1.46	0.198	3.45	1.29	0.518	0.162
0.55	7.5	126.89	0.835	1.31	0.187	2.66	1.46	0.128	0.252
0.6	7.22	128.81	3.86	1.13	0.167	1.69	1.46	0.368	0.27
0.65	3.9	130.65	6.83	0.93	0.149	0.614	1.31	0.755	0.217
0.7	3.75	132.25	9.72	0.729	0.154	0.507	1.01	1.04	0.126
0.75	1.72	135.29	15.2	0.365	0.214	2.57	0.179	1.13	0.169
0.8	6.16	137.77	20.2	0.153	0.253	3.82	0.651	0.454	0.229
0.85	7.5	139.85	24.6	0.051	0.187	3.95	1.14	0.499	0.141
0.9	5.09	141.45	28.2	0.246	0.071	2.84	1.1	1.11	0.178

Figure 14. Performance varies with different pole arc coefficient: (**a**) cogging torque; and (**b**) spectrum for the back EMFs in all phases.

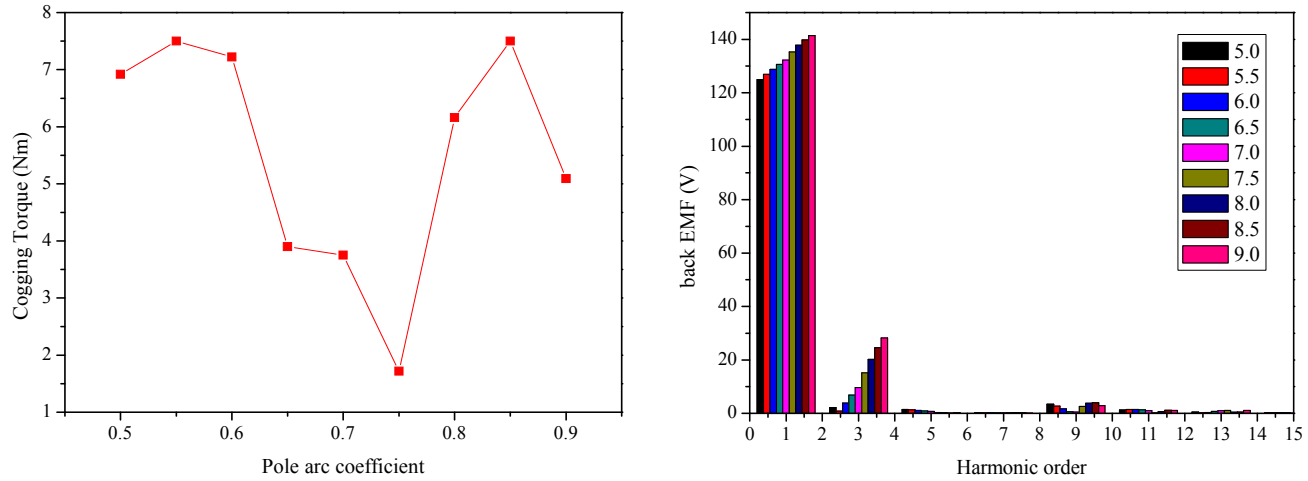

(**a**) (**b**)

3.3. Short Circuit Current Constraint

Winding short-circuit fault is the most severe failure that might occur in the stator windings. Conventional permanent magnet machines possess a short-circuit current that is several times higher than the rated stator current. Therefore, the short-circuit fault will overheat the stator conductors and bring about deterioration situations further.

The alternate-teeth-wound fractional-slot concentrated winding PMSM provides an inherent thermal isolation feature of the stator phase windings. Besides, all of the phases windings are magnetically isolated, signifying that the short-circuit fault in certain phase windings will not interfere the other phases. If only we restrain the short-circuit current within about 1.0 per unit, the motor can be prevented from the potential damage caused by the short-circuit current. The leakage inductance of a fractional-slot concentrated winding PMSM consists of harmonic leakage inductance, slot leakage inductance and end leakage inductance, which is quite large compare with the one with distributed windings [38]. The main MMF component corresponding to the mechanical-electrical energy conversion is usually a high order MMF component. For instance, the main MMF component is the

11th one for a 24-slot/22-pole fractional-slot concentrated winding machine. It can be calculated that the harmonic leakage inductance could be several times larger than the main inductance by the analyses provided in references [19,20]. Along with the slot leakage inductance, the self-inductance of the fractional-slot concentrated winding machine could be rather large in contrast to the distributed winding machine.

It should be noted that, the inner power factor of the machine declines although a lower short-circuit current can be achieved with large leakage inductance. The vector diagram of the equivalent circuit in d-q reference frame for PMSM with 1.0 per unit short-circuit current is illustrated in Figure 15.

Figure 15. Vector diagram for PMSM with 1.0 per unit short-circuit current: (**a**) short circuit; and (**b**) normal condition.

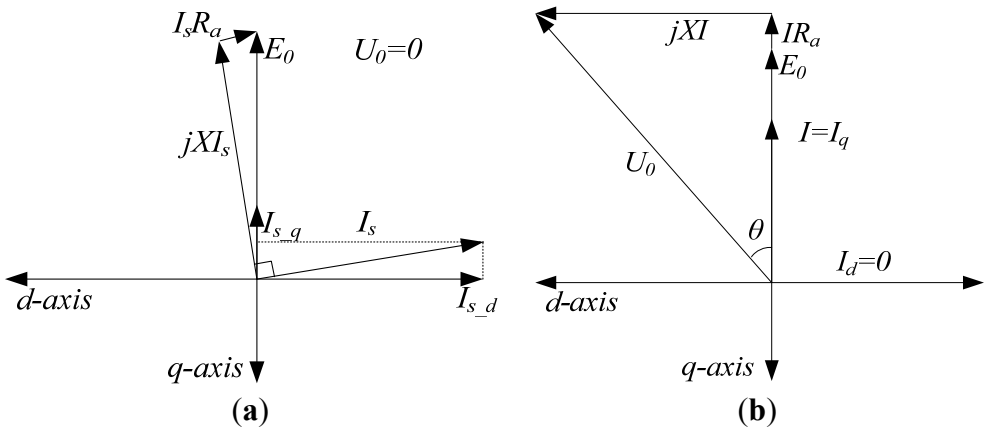

As can be seen in Figure 15a, the relationship of the vectors in case of the short-circuit fault can be written as:

$$E_0 = \sqrt{(I_s X)^2 + (I_s R_a)^2} \tag{3}$$

where the E_0 is back EMF; I_s is the short-circuit current; X is the reactance of the stator winding; and R_a is the resistance of the winding. Since the resistance of the winding is negligible compared to the winding reactance, Equation (2) can be reduced to:

$$E_0 = I_s X \tag{4}$$

Thus, the angle between the phase voltage vector U_0 and stator current I with I_d = 0 control is given by:

$$\theta = arc\tan\left(\frac{XI}{E_0 + I_s R_a}\right) \tag{5}$$

where the stator current I equals the short-circuit current I_s. The winding resistance R_a can be disregarded again, then:

$$\theta = arc\tan\left(\frac{XI}{E_0 + I_s R_a}\right) = arc\tan 1 = 45^\circ \tag{6}$$

Therefore, the inner power factor is given by:

$$\theta = \cos 45^\circ = 0.707 \tag{7}$$

Although the inner power factor is quite low under $I_d = 0$ control, the actual power factor can be adjusted by changing the stator current vector I.

3.4. Optimal Scheme

Combing the above analyses of optimal coil-wound tooth tip span, pole arc coefficient and short-circuit current constraint mentioned in Sections 3.2 and 3.3, the key parameters for the optimal scheme are shown in Table 7 and Figure 16. To achieve the desired power, voltage and the other parameters, an analytical design program was firstly performed to calculate, adjust and obtain the sensible but relatively rough parameters [39]. After that, FEA methods are employed to check and adjust the desired power, voltage, efficiency, *etc.* Therefore, an accurate design is achieved.

Table 7. Key parameters and dimensions of the optimal scheme.

Parameters	Units	Values
Inner diameter of stator	mm	212
Outer diameter of stator	mm	320
Outer diameter of rotor	mm	360
Air gap length	mm	1
Slot opening	mm	4.0
Stack length	mm	40
Magnet height	mm	5
Pole arc coefficient	-	0.9
Material of PMs	-	N45SH (B_r = 1.35T)
Maximum current	A_{pk}	30
Current density	A/mm^2	10.10
One-phase short circuit current	A_{pk}	29.01
Slot fill factor	%	70.25
Number of conductors per slot	-	110
Maximum torque@450 rpm	Nm	250.57
Torque ripple	%	6.56%
1-st component of back EMF@450 rpm	V	143.75
Rated/Maximum power	kW	12/24
Active power-to-mass density	kW/kg	1.415

Figure 16. The optimal design scheme: (**a**) assembly; and (**b**) modular stator.

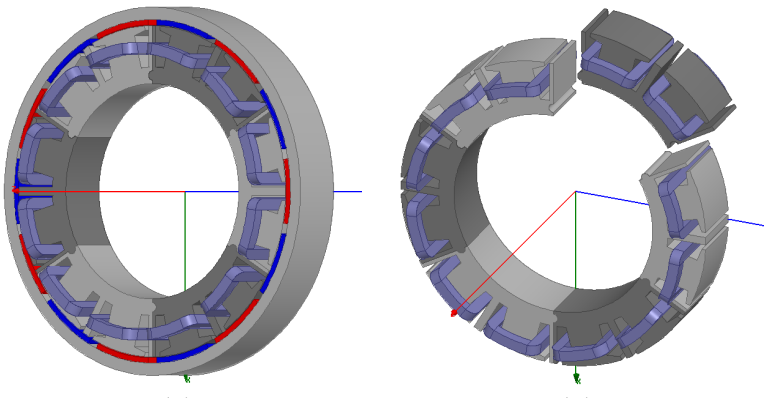

(**a**) (**b**)

Besides, circumferential segmentation of the rotor PMs is employed to restrain the eddy current within short paths [40]. For the PM material of N45SH, the relative permeability μ_r = 1.113 and the conductivity ρ = 160 μΩ·cm. Thus, the depth of penetration is calculated as 1.5 cm. Each piece of the PM is divided into four parts to reduce the eddy current loss.

The proposed outer rotor 24-slot/14-pole machine is designed for the in-wheel driving applications. The machine has a maximum speed of 1200 rpm and maximum torque of 250 Nm. For the constrain of DC-bus voltage of 288 V, the flux-weakening operation is applied to expand the speed to 1200 rpm. The efficiencies in all speed ranges are shown in Figure 17. Iron losses, joule losses and estimated mechanical losses are taken into consideration. The current regulation is based on the control strategy of maximum torque per ampere (MTPA).

As can be seen in Figure 17, the efficiency reaches the maximum value of 0.95. The area where the efficiency is greater than 0.90 covers approximately 78.2% of the whole region. The area where efficiency is greater than 0.80 accounts for 87.5%, which shows that the designed machine is high-efficient in most operating area. The presented design could be an interesting candidate for prototyping.

Figure 17. Efficiency map in all speed ranges.

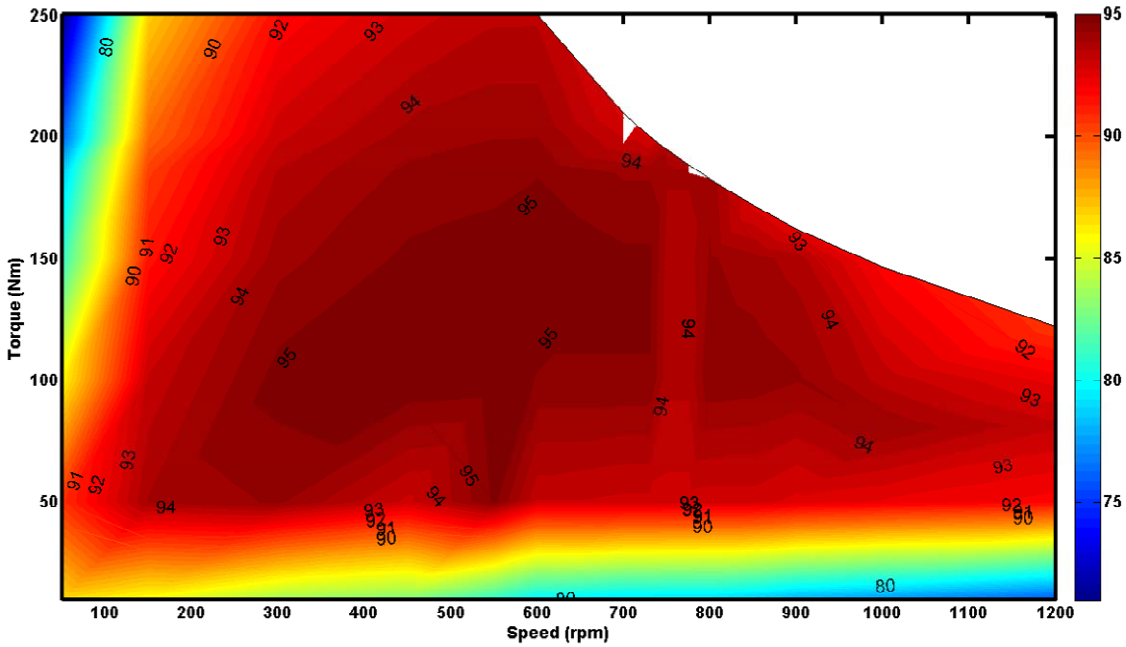

4. Conclusions

(1) A novel 24-slot/14-pole PMSM adopting alternate-teeth-wound FSCWs and unequal teeth widths is proposed for in-wheel application, with the advantages of completely isolation features and reduced MMF harmonics;

(2) The magnetic isolation feature of the proposed alternate-teeth-wound 24-slot/14-pole six-phase PMSM having two adjacent coils per phase is superior to the alternate-teeth-wound 24-slot/22-pole scheme which is a conventional optimal choice;

(3) A 24 kW outer rotor prototype machine is designed and optimized using the FEA method. The modular stator core is form of six armature cores which provides the convenient features of easy fabrication and post-fault replacement. The defect of lower winding factor regarding the proposed

machine is solved by extending the tooth tip span of the coil-wound teeth. The winding leakage inductance is utilized to restrain the winding short circuit current to nearly 1.0 per unit but with low inner power factor;

(4) An optimal design scheme with high winding factor, 1.0 per unit short circuit current, high efficiency in all speed ranges is obtained and presented for in-wheel application;

(5) In order to obtain flexibilities of post-fault control, the proposed solution imposes twelve legs instead of six legs for dual-three phase windings resulting in high cost of the power converter, which should be considered in future work.

Acknowledgments

This work was supported in part by the 863 Plan of China under Project 2011AA11A261, in part by National Natural Science Foundation of China under Project 51077026, and in part by the Fundamental Research Funds for the Central Universities (Grant No. HIT.BRET1.2010013).

Conflicts of Interest

The authors declare no conflict of interest.

References

1. Wang, J.; Yuan, X.; Atallah, K. Design optimization of a surface-mounted permanent-magnet motor with concentrated windings for electric vehicle applications. *IEEE Trans. Veh. Technol.* **2013**, *62*, 1053–1064.
2. Nikam, S.P.; Rallabandi, V.; Fernandes, B.G. A high-torque-density permanent-magnet free motor for in-wheel electric vehicle application. *IEEE Trans. Ind. Appl.* **2012**, *48*, 2287–2295.
3. Wang, J.; Atallah, K.; Zhu, Z.Q.; Howe, D. Modular three-phase permanent-magnet brushless machines for in-wheel applications. *IEEE Trans. Veh. Technol.* **2008**, *57*, 2714–2720.
4. Jack, A.G.; Mecrow, B.C.; Haylock, J.A. A comparative study of permanent magnet and switched reluctance motors for high-performance fault-tolerant applications. *IEEE Trans. Ind. Appl.* **1996**, *32*, 889–895.
5. Fasolo, A.; Alberti, L.; Bianchi, N. Performance Comparison between Switching-Flux and IPM Machine with Rare Earth and Ferrite PMs. In Proceedings of the XXth IEEE International Conference on Electric Machines (ICEM), Marseille, France, 2–5 September 2012; pp. 731–737.
6. Campos-Delgado, D.U.; Espinoza-Trejo, D.R.; Palacios, E. Fault-tolerant control in variable speed drives: A survey. *IET Electr. Power Appl.* **2008**, *2*, 121–134.
7. Mecrow, B.C.; Jack, A.G.; Haylock, J.A.; Coles, J. Fault tolerant permanent magnet machine drives. *IEE Proc. Electr. Power Appl.* **1996**, *143*, 437–442.
8. El-Refaie, A.M. Fault-tolerant permanent magnet machines: A review. *IET Electr. Power Appl.* **2011**, *5*, 59–74.
9. Chung, S.-U.; Kim, J.-M.; Koo, D.-H.; Woo, B.-C.; Hong, D.-K.; Lee, J.-Y. Fractional slot concentrated winding permanent magnet synchronous machine with consequent pole rotor for low speed direct drive. *IEEE Trans. Magn.* **2012**, *48*, 2965–2968.

10. Reddy, P.B.; EL-Refaie, A.M.; Huh, K.-K.; Tangudu, J.K.; Jahns, T.M. Comparison of interior and surface PM machines equipped with fractional-slot concentrated windings for hybrid traction applications. *IEEE Trans. Energy Convers.* **2012**, *27*, 593–602.
11. EL-Refaie, A.M. Fractional-slot concentrated-windings synchronous permanent magnet machines: Opportunities and challenges. *IEEE Trans. Ind. Electron.* **2010**, *57*, 107–121.
12. Chen, J.T.; Zhu, Z.Q. Winding configurations and optimal stator and rotor pole combination of flux-switching PM brushless AC machines. *IEEE Trans. Energy Convers.* **2010**, *25*, 293–302.
13. Ishak, D.; Zhu, Z.Q.; Howe, D. Permanent-magnet brushless machines with unequal tooth widths and similar slot and pole numbers. *IEEE Trans. Ind. Appl.* **2005**, *41*, 584–590.
14. Welchko, B.A.; Lipo, T.A.; Jahns, T.M.; Schulz, S.E. Fault tolerant three-phase AC motor drive topologies: A comparison of features, cost, and limitations. *IEEE Trans. Power Electron.* **2004**, *19*, 1008–1116.
15. Abolhassani, M.T.; Toliyat, H.A. Fault Tolerant Permanent Magnet Motor Drives for Electric Vehicles. In Proceedings of the IEEE International Conference on Electric Machines and Drives, Miami, FL, USA, 3–5 May 2009; pp. 1146–1152.
16. Jussila, H.; Salminen, P.; Niemela, M.; Pyrhonen, J. Guidelines for Designing Concentrated Winding Fractional Slot Permanent Magnet Machines. In Proceedings of the International Conference on Power Engineering, Setubal, Portugal, 12–14 April 2007; pp. 191–194.
17. Reddy, P.B.; Jahns, T.M.; EL-Refaie, A.M. Impact of Winding Layer Number and Slot/Pole Combination on AC Armature Losses of Synchronous Surface PM Machines Designed for Wide Constant-Power Speed Range Operation. In Proceedings of the IEEE Industry Applications Society Annual Meeting (IAS), Edmonton, AB, Canada, 5–9 October 2008; doi:10.1109/08IAS.2008.57.
18. Bianchi, N.; Bolognani, S.; Pre, M.D.; Grezzani, G. Design considerations for fractional-slot winding configurations of synchronous machines. *IEEE Trans. Ind. Appl.* **2006**, *42*, 997–1006.
19. EL-Refaie, A.M.; Zhu, Z.Q.; Jahns, T.M.; Howe, D. Winding Inductances of Fractional Slot Surface-Mounted Permanent Magnet Brushless Machines. In Proceedings of the IEEE Industry Applications Society Annual Meeting (IAS), Edmonton, AB, Canada, 5–9 October 2008; doi:10.1109/08IAS.2008.61.
20. Zheng, P.; Wu, F.; Sui, Y.; Wang, P.; Lei, Y.; Wang, H. Harmonic analysis and fault-tolerant capability of a semi-12-phase permanent-magnet synchronous machine used for EVs. *Energies* **2012**, *5*, 3586–3607.
21. Tangudu, J.K.; Jahns, T.M.; Bohn, T.P. Design, Analysis and Loss Minimization of a Fractional-Slot Concentrated Winding IPM Machine for Traction Applications. In Proceedings of the IEEE Energy Conversion Congress and Exposition, Phoenix, AZ, USA, 17–22 September 2011; pp. 2236–2243.
22. Reddy, P.B.; Jahns, T.M.; McCleer, P.J.; Bohn, T.P. Design, Analysis and Fabrication of a High Performance Fractional-Slot Concentrated Winding Surface PM Machine. In Proceedings of the IEEE Energy Conversion Congress and Exposition, Atlanta, GA, USA, 12–16 September 2010; pp. 1074–1081.

23. Brown, N.R.; Jahns, T.M.; Lorenz, R.D. Power Converter Design for an Integrated Modular Motor Drive. In Proceedings of the IEEE 42nd Industry Applications Conference (IAS) Annual Meeting, New Orleans, LA, USA, 23–27 September 2007; pp. 1322–1328.
24. Ouyang, W.; Huang, S.; Good, A.; Lipo, T.A. Modular Permanent Magnet Machine Based on Soft Magnetic Composite. In Proceedings of the IEEE International Conference on Electric Machines and Drives, Nanjing, China, 27–29 September 2005; pp. 235–239.
25. Dwari, S.; Parsa, L.; Lipo, T.A. Optimum Control of a Five-Phase Integrated Modular Permanent Magnet Motor under Normal and Open-Circuit Fault Conditions. In Proceedings of the IEEE Power Electronics Specialists Conference, Orlando, FL, USA, 17–21 June 2007; pp. 1639–1644.
26. Griva, G.; Oleschuk, V. Neutral-Point-Clamped Inverters with Hybrid PWM for Symmetrical Six-Phase Motor Drive. In Proceedings of the 35th Annual Conference of the IEEE Industrial Electronics Society, Porto, Portugal, 3–5 November 2009; pp. 658–663.
27. Prieto, J.; Barrero, F.; Lim, C.S.; Levi, E. Predictive Current Control with Modulation in Asymmetrical Six-Phase Motor Drives. In Proceedings of the IEEE Power Electronics and Motion Control Conference, Novi Sad, Serbia, 4–6 September 2012; pp. LS1c.1-1–LS1c.1-8.
28. Klingshirn, E.A. High phase order induction motors—Parts I and II. *IEEE Trans. Power Appar. Syst.* **1983**, *102*, 47–59.
29. Barcaro, M.; Bianchi, N.; Magnussen, F. Six-phase supply feasibility using a pm fractional-slot dual winding machine. *IEEE Trans. Ind. Appl.* **2011**, *47*, 2042–2050.
30. Magnussen, F.; Sadarangani, C. Winding Factors and Joule Losses of Permanent Magnet Machines with Concentrated Windings. In Proceedings of the IEEE International Electric Machines and Drives Conferences, Madison, WI, USA, 1–4 June 2003; pp. 333–339.
31. Fornasiero, E.; Bianchi, N.; Bolognani, S. Slot harmonic impact on rotor losses in fractional-slot permanent-magnet machines. *IEEE Trans. Ind. Electron.* **2012**, *59*, 2557–2564.
32. Bianchi, N.; Fornasiero, E. Impact of MMF space harmonic on rotor losses in fractional-slot permanent-magnet machines. *IEEE Trans. Energy Convers.* **2009**, *24*, 323–328.
33. Cros, J.; Viarouge, P. Synthesis of high performance PM motors with concentrated windings. *IEEE Trans. Energy Convers.* **2002**, *17*, 248–253.
34. Cros, J.; Matte, D.; Viarouge, P. Multi Phase Electrical Motor for Use in a Wheel. European Patent 1943715 A1, 16 July 2008.
35. Dube, J.; Cros, J.; Viarouge, P. High Performance Brushless Motor and Drive for an Electrical Vehicle Motorization. U.S. Patent 6888280 B2, 3 May 2005.
36. Atallah, K.; Wang, J.; Howe, D. Torque-ripple minimization in modular permanent-magnet brushless machines. *IEEE Trans. Ind. Appl.* **2003**, *39*, 1689–1695.
37. Ouyang, W. Modular Permanent Magnet Machine Drive System with Fault Tolerant Capability. Ph. D. Thesis, University of Wisconsin-Madison, Madison, WI, USA, 2007; pp. 27–36.
38. Ponomarev, P.; Lindh, P.; Pyrhonen, J. Effect of slot and pole combination on the leakage inductance and the performance of tooth-coil permanent-magnet synchronous machines. *IEEE Trans. Ind. Electron.* **2012**, *60*, 1–8.
39. Lipo, T.A. *Introduction to AC Machine Design*, 3rd ed.; Wisconsin Power Electronics Research Center, University of Wisconsin: Madison, WI, USA, 2007; pp. 447–562.

40. Aslan, B.; Semail, E.; Legranger, J. Analytical Model of Magnet Eddy-Current Volume Losses in Multi-Phase PM Machines with Concentrated Winding. In Proceedings of the IEEE Energy Conversion Congress and Exposition, Raleigh, NC, USA, 15–20 September 2012; pp. 3371–3378.